RESEARCH BRIEF

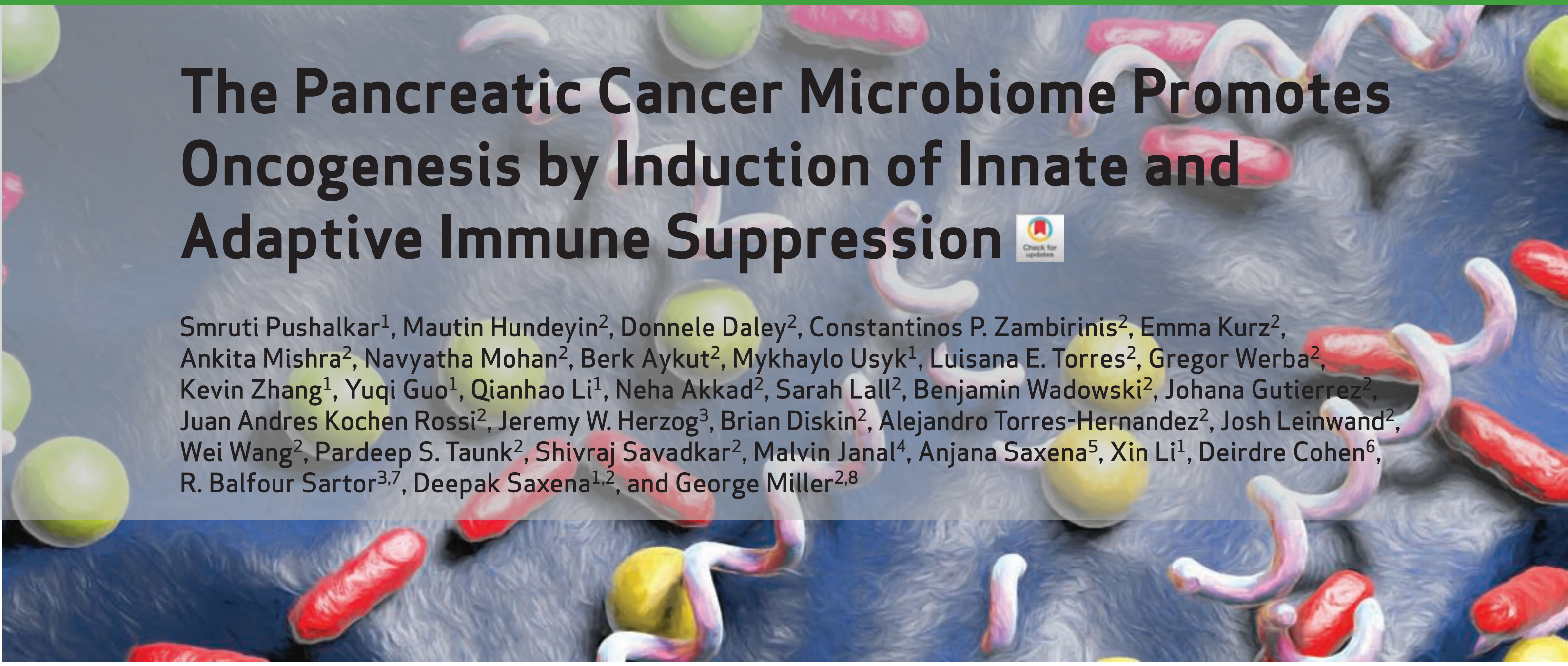

The Pancreatic Cancer Microbiome Promotes Oncogenesis by Induction of Innate and Adaptive Immune Suppression

Smruti Pushalkar[1], Mautin Hundeyin[2], Donnele Daley[2], Constantinos P. Zambirinis[2], Emma Kurz[2], Ankita Mishra[2], Navyatha Mohan[2], Berk Aykut[2], Mykhaylo Usyk[1], Luisana E. Torres[2], Gregor Werba[2], Kevin Zhang[1], Yuqi Guo[1], Qianhao Li[1], Neha Akkad[2], Sarah Lall[2], Benjamin Wadowski[2], Johana Gutierrez[2], Juan Andres Kochen Rossi[2], Jeremy W. Herzog[3], Brian Diskin[2], Alejandro Torres-Hernandez[2], Josh Leinwand[2], Wei Wang[2], Pardeep S. Taunk[2], Shivraj Savadkar[2], Malvin Janal[4], Anjana Saxena[5], Xin Li[1], Deirdre Cohen[6], R. Balfour Sartor[3,7], Deepak Saxena[1,2], and George Miller[2,8]

ABSTRACT

We found that the cancerous pancreas harbors a markedly more abundant microbiome compared with normal pancreas in both mice and humans, and select bacteria are differentially increased in the tumorous pancreas compared with gut. Ablation of the microbiome protects against preinvasive and invasive pancreatic ductal adenocarcinoma (PDA), whereas transfer of bacteria from PDA-bearing hosts, but not controls, reverses tumor protection. Bacterial ablation was associated with immunogenic reprogramming of the PDA tumor microenvironment, including a reduction in myeloid-derived suppressor cells and an increase in M1 macrophage differentiation, promoting TH1 differentiation of CD4$^+$ T cells and CD8$^+$ T-cell activation. Bacterial ablation also enabled efficacy for checkpoint-targeted immunotherapy by upregulating PD-1 expression. Mechanistically, the PDA microbiome generated a tolerogenic immune program by differentially activating select Toll-like receptors in monocytic cells. These data suggest that endogenous microbiota promote the crippling immune-suppression characteristic of PDA and that the microbiome has potential as a therapeutic target in the modulation of disease progression.

SIGNIFICANCE: We found that a distinct and abundant microbiome drives suppressive monocytic cellular differentiation in pancreatic cancer via selective Toll-like receptor ligation leading to T-cell anergy. Targeting the microbiome protects against oncogenesis, reverses intratumoral immune tolerance, and enables efficacy for checkpoint-based immunotherapy. These data have implications for understanding immune suppression in pancreatic cancer and its reversal in the clinic. *Cancer Discov; 8(4);1–14. ©2018 AACR.*

---

[1]Department of Basic Science and Craniofacial Biology, New York University College of Dentistry, New York, New York. [2]S. Arthur Localio Laboratory, Department of Surgery, New York University School of Medicine, New York, New York. [3]National Gnotobiotic Rodent Research Center, University of North Carolina, Chapel Hill, North Carolina. [4]Department of Epidemiology and Health Promotion, NYU College of Dentistry, New York, New York. [5]Department of Biology, Brooklyn College and the Graduate Center (CUNY), Brooklyn, New York, New York. [6]Department of Medicine, New York University School of Medicine, New York, New York. [7]Department of Medicine, Microbiology, and Immunology, University of North Carolina, Chapel Hill, North Carolina. [8]Department of Cell Biology, New York University School of Medicine, New York, New York.

Note: Supplementary data for this article are available at Cancer Discovery Online (http://cancerdiscovery.aacrjournals.org/).

S. Pushalkar, M. Hundeyin, and D. Daley contributed equally to this article.

D. Saxena and G. Miller share senior authorship of this article.

Corresponding Authors: George Miller, New York University School of Medicine, 430 East 29th Street, Suite 660, New York, NY 10016. Phone: 646-501-2208; Fax: 646-501-4564; E-mail: george.miller@nyumc.org; and Deepak Saxena, Department of Basic Science and Craniofacial Biology, New York University College of Dentistry, 345 East 24th Street, Room 921B, New York, NY 10010. Phone: 212-998-9256; E-mail: ds100@nyu.edu

doi: 10.1158/2159-8290.CD-17-1134

INTRODUCTION

Pancreatic ductal adenocarcinoma (PDA) is the third most lethal cancer in the United States and accounts for 85% of all pancreatic malignancies (1). Peripancreatic inflammation is paramount for induction of oncogenesis. Innate and adaptive immune cell subsets cooperate through various mechanisms to promote tumorigenesis. We previously reported that activation of pattern recognition receptors (PRR), which transmit inflammation in response to microbial pathogens, accelerates tumorigenesis, whereas mice deficient in select PRR signaling [including Toll-like receptor 4 (TLR4), TLR7, TLR9, and Mincle] exhibit slower progression of PDA (2–6). The protumorigenic effects of PRR ligation in PDA are mediated through multiple mechanisms, including induction of innate and adaptive immune suppression, activation of protumorigenic signaling pathways such as NF-κB, Notch, and STAT3, and activation of fibrogenic cells in the PDA tumor microenvironment (2–5). Based on these data, we postulated that bacterial dysbiosis influences PDA progression.

Both microbial dysbiosis and disrupted epithelial barrier function leading to translocation of bacteria are thought to be inducing factors in neoplastic transformation (7). The microbiome has emerged as a contributor to oncogenesis in a number of intestinal tract malignancies, including laryngeal, esophageal, gastric, and colorectal cancers, as well as in primary liver cancer (8). In the aforementioned malignancies, the gut microbiome is in direct contact with the at-risk organ or, in the case of liver cancer, the recipient of portal venous drainage from the intestine. However, very few reports implicate the gut microbiome in carcinomas ostensibly remote from the gastrointestinal lumen or its drainage (9, 10). Moreover, the etiologic relationship between the intrapancreatic microbiota and immune-suppressive inflammation in PDA has not been described.

We found that PDA is associated with a distinct stage-specific gut and pancreatic microbiome that drives disease progression by inducing intratumoral immune suppression. Conversely, targeting the microbiome markedly protected against PDA and enhanced antitumor immunity and susceptibility to immunotherapy. Our data suggest that elements of the microbiome may be useful in early diagnosis and risk stratification. Further, microbial-targeted therapies may reduce risk in preinvasive disease and may be used as an adjuvant to standard therapies or in synergy with checkpoint-directed immunotherapy in invasive disease.

RESULTS

To determine whether endoluminal gut bacteria access the pancreas, we administered fluorescently labeled *Enterococcus faecalis* to wild-type (WT) mice via oral gavage. Bacteria migrated into the pancreas, suggesting that intestinal bacteria can directly influence the pancreatic microenvironment (Fig. 1A). Similar findings were observed using GFP-labeled *Escherichia coli* (Fig. 1B). 16S rRNA FISH indicated a markedly greater presence of bacteria in both mouse and human PDA compared with normal pancreas (Fig. 1C and D). qPCR analysis confirmed increased bacterial abundance in PDA compared with normal pancreas in mice and humans (Fig. 1E and F). Repopulation experiments in antibiotic-treated WT mice suggested that the gut microbiome from *Pdx1*$^{\text{Cre}}$;LSL-*Kras*$^{\text{G12D}}$;*Trp53*$^{\text{R172H}}$ (KPC) mice has a higher capacity for translocation to the pancreas compared with WT gut microbiome (Fig. 1G). Notably, *Agrobacterium* and *Rhizobium*, which are associated with mouse chow, were among the most abundant genera in both the WT mouse pancreas and the *Ptf1a*$^{\text{Cre}}$;LSL-*Kras*$^{\text{G12D}}$ (KC) pancreas, further suggesting translocation (Supplementary Fig. S1A). To characterize the human intrapancreatic microbiome, we performed 16S rRNA gene sequencing on PDA tumors from 12 patients. Thirteen distinct phyla were detected in human PDA. *Proteobacteria* (45%), *Bacteroidetes* (31%), and *Firmicutes* (22%) were most abundant and were prevalent in all samples (Supplementary Fig. S1B). *Actinobacteria* (1%) was also prevalent in all samples. Genera *Pseudomonas* and *Elizabethkingia* were highly abundant and prevalent in all human PDA specimens (Supplementary Fig. S1C). The bacterial composition in human PDA was distinct from that of normal human pancreas, based on assessment of clade abundances using linear discriminant analysis effect size (LEfSe; Supplementary Fig. S1D).

To determine whether bacteria promote the progression of pancreatic dysplasia, we used the slowly progressive KC model of pancreatic oncogenesis. Germ-free KC mice were protected against disease progression and stromal expansion. Compared with age-matched control KC mice, germ-free cohorts exhibited delayed acinar effacement, reduced pancreatic dysplasia, diminished intratumoral fibrosis, and lower pancreatic weights (Fig. 1H–J). Similarly, in an invasive orthotopic PDA model using KPC-derived tumor cells, WT mice treated with an ablative oral antibiotic regimen developed ~50% reduced tumor burdens (Fig. 1K). Bacterial ablation was similarly

Figure 1. The tumorous pancreas has an abundant microbiome and its ablation is protective against pancreatic disease progression. **A,** WT mice were administered CFSE-labeled *E. faecalis* [2.5×10^8 colony-forming units (CFU)] via oral gavage. Pancreata were harvested and digested at the indicated timed intervals and tested for the presence of these bacteria ($n = 3$ mice/time point). This experiment was repeated twice with similar results. **B,** WT mice were administered GFP-labeled *E. coli* (2.5×10^8 CFU) via oral gavage. Pancreata were harvested at 6 hours, and the number of GFP$^+$ foci was determined by immune fluorescence microscopy compared with control. This experiment was repeated twice ($n = 3$; **, $P < 0.01$; scale bar, 50 μm). HPF, high-power field. **C,** The abundance of intrapancreatic bacteria was compared in 3-month-old WT and KC mice by FISH ($n = 5$/group). Representative images are shown. This experiment was repeated twice. **D,** The abundance of intrapancreatic bacteria was compared in healthy individuals and age/gender/body mass index (BMI)–matched patients with PDA by FISH ($n = 5$/group). Representative images are shown. **E,** Bacterial DNA content was compared in WT and KC mice using qPCR. Each dot represents data from a single mouse pancreas. This was repeated three times (**, $P < 0.01$). **F,** Bacterial DNA content was compared in healthy individuals (NML) and age/gender/BMI-matched patients with PDA using qPCR. Each dot represents data from a single human pancreas (****, $P < 0.0001$). **G,** Eight-week-old WT mice were treated with an ablative oral antibiotic regimen. Three weeks after treatment, mice were repopulated using fecal bacteria from either 3-month-old WT or KPC mice. Bacterial colonization of the pancreas was analyzed by qPCR 2 weeks after repopulation. This experiment was repeated twice ($n = 5$/group; *, $P < 0.05$). **H–J,** Control and germ-free (GF) KC mice were sacrificed at 3, 6, or 9 months of life. Representative (**H**) hematoxylin and eosin (H&E)– and (**I**) trichrome-stained sections are shown. The percentage of ducts exhibiting normal morphology, acinoductal metaplasia (ADM), or graded PanIN lesions were determined based on H&E staining. The fraction of fibrotic area per pancreas was calculated based on trichrome staining (scale bars, 200 μm). **J,** Pancreatic weights were recorded at 3 or 6 months of life ($n = 10$/group; *, $P < 0.05$; **, $P < 0.01$; ***, $P < 0.001$; ****, $P < 0.0001$). **K,** WT mice were treated with an ablative oral antibiotic regimen (Abx) and then orthotopically inoculated with KPC-derived PDA cells. Animals were sacrificed at 3 weeks, and tumor weights were recorded ($n = 4$/group; **, $P < 0.01$). This experiment was repeated more than 5 times with similar results.

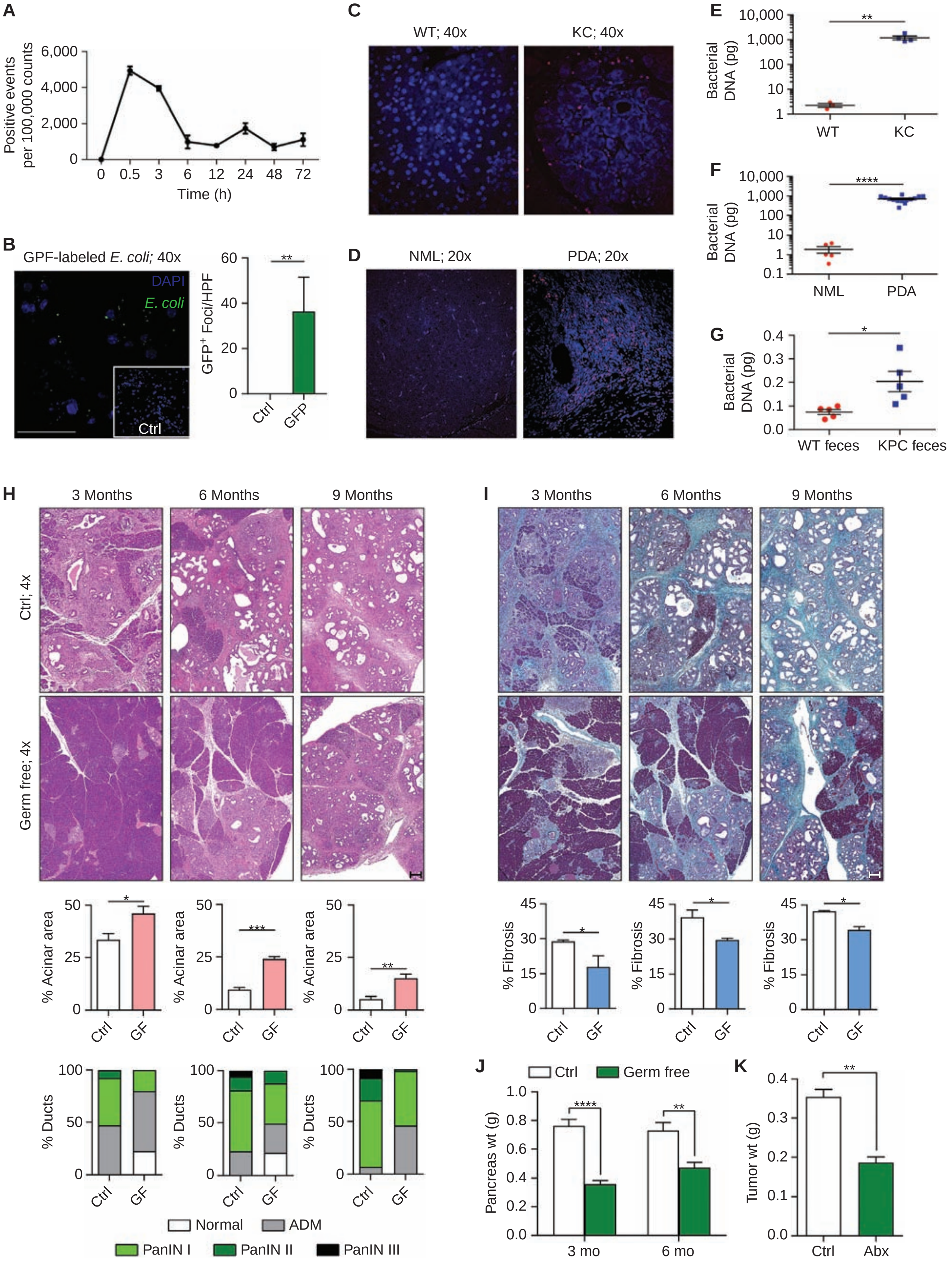
A
Positive events per 100,000 counts
6,000
4,000
2,000
0
0 0.5 3 6 12 24 48 72
Time (h)
B
GPF-labeled *E. coli;* 40x
DAPI
E. coli
Ctrl
GFP$^+$ Foci/HPF
60
40
20
0
**
Ctrl
GFP
C
WT; 40x
KC; 40x
D
NML; 20x
PDA; 20x
E
Bacterial DNA (pg)
10,000
1,000
100
10
1
**
WT
KC
F
Bacterial DNA (pg)
10,000
1,000
100
10
1
0.1
****
NML
PDA
G
Bacterial DNA (pg)
0.4
0.3
0.2
0.1
0.0
*
WT feces
KPC feces
H
3 Months
6 Months
9 Months
Ctrl; 4x
Germ free; 4x
% Acinar area
50
25
0
*
***
**
Ctrl
GF
% Ducts
100
50
0
Normal
ADM
PanIN I
PanIN II
PanIN III
I
3 Months
6 Months
9 Months
% Fibrosis
45
30
15
0
*
*
*
Ctrl
GF
J
Ctrl
Germ free
Pancreas wt (g)
1.0
0.8
0.6
0.4
0.2
0.0
****
**
3 mo
6 mo
K
Tumor wt (g)
0.4
0.3
0.2
0.1
0.0
**
Ctrl
Abx

protective when using *Kras* WT Pan02 cells (Supplementary Fig. S1E). These data imply that bacteria promote the progression of pancreatic oncogenesis in both preinvasive and invasive models. We confirmed that our oral antibiotic regimen ablated the pancreatic microbiome (Supplementary Fig. S1F).

To identify longitudinal perturbations in the microbiome associated with temporal progression of pancreatic dysplasia, we serially interrogated fecal bacterial profiles in KC and WT mice over a period of 9 months using 16S rRNA sequencing. Early in murine life, gut bacterial community structures in KC and WT cohorts were similar. *Bacteroidetes* and *Firmicutes* were the dominant phyla, but no significant differences were observed between cohorts. However, although *Actinobacteria* were present in low abundance in young WT and KC mice, they increased to ~60% abundance in the KC cohorts by week 20. Conversely, *Actinobacteria* did not expand in the WT cohort. *Deferribacteres* also increased abruptly in KC mice in weeks 28 to 36 (Supplementary Fig. S2A). At the genus level, the KC gut microbiome clustered separately from WT after week 13 (Supplementary Fig. S2B). Longitudinal comparisons of gut microbial communities in KC mice suggested an enrichment of *Bifidobacterium* at later time points (Supplementary Fig. S2C). Linear discriminant analysis (LDA) similarly showed that *Bifidobacterium* was progressively enriched in the KC cohort compared with WT from weeks 13 to 36 (Supplementary Fig. S2D). We found that *Bifidobacterium pseudolongum* was the most abundant *Bifidobacterium* species in KC mice (Supplementary Fig. S2E). Principal coordinate analysis (PCoA) computed using weighted UniFrac distance metrics confirmed distinct differences in gut microbial communities between WT and KC cohorts at select time points (Supplementary Fig. S2F and S2G). Alpha diversity analyses further suggested significant differences in taxonomy-based richness (Chao1), observed operational taxonomic units (OTU), Shannon diversity index, and phylogeny-based diversity (PD) in the KC cohort with progressive oncogenesis (Supplementary Fig. S3A–S3D). Alpha diversity in gut microbial communities was also distinct between WT and KC cohorts (Supplementary Fig. S3E–S3H).

Because we showed that bacteria can migrate from the gut to the pancreas, we evaluated bacterial membership and structure in fecal samples of patients with PDA (PDA; $n = 32$) compared with matched healthy individuals (NML; $n = 31$). At the phylum level, the gut microbiota of patients with PDA and controls were each similarly dominated by *Firmicutes* and *Bacteroidetes* (Supplementary Fig. S4A). However, *Proteobacteria, Synergistetes,* and *Euryarchaeota* were significantly more abundant in patients with PDA compared with healthy subjects. Notably, whereas *Proteobacteria* comprised only ~8% of gut bacteria in patients with PDA (Supplementary Fig. S4A), this phyla constituted nearly 50% abundance in the cancerous pancreas (Supplementary Fig. S1B). Direct comparison of the gut and pancreas microbiomes in patients with PDA for which both fecal and tumor samples were available indicated differentially increased translocation of gram-negative *Proteobacteria* to the pancreas (Supplementary Fig. S4B). *Pseudomonas* and *Elizabethkingia* were the most abundant *Proteobacteria* genera in PDA, whereas *Prevotella* and *Bacteroides* were more abundant in the gut (Supplementary Fig. S4C). Comparison of the pancreas and duodenal microbiomes in KC mice also indicated enrichment of select gram-negative bacteria in the pancreas (Supplementary Fig. S4D). LDA analysis suggested that numerous genera belonging to *Firmicutes, Proteobacteria, Actinobacteria,* and *Bacteroidetes* were expanded in the gut in human PDA (Supplementary Fig. S5A). Alpha diversity measures assessing the human gut microbiome suggested differences between NML and PDA cohorts based on the abundance-based coverage estimator (ACE), Chao1, observed OTUs, Shannon, Simpson, and PD indices (Supplementary Fig. S5B).

To test whether pathogenic bacteria promote pancreatic oncogenesis in genetically susceptible hosts, we ablated gut bacteria in KC mice using oral antibiotics and then selectively repopulated cohorts using feces derived from either WT mice or KPC mice before sacrifice at 22 weeks of life (Supplementary Fig. S6A). Consistent with our previous results, bacterial ablation was protective against disease progression (Fig. 2A). Further, repopulation using KPC-derived feces accelerated tumor growth to baseline levels whereas repopulation with feces from age-matched WT mice failed to significantly accelerate tumorigenesis (Fig. 2A). Similarly, in the germ-free KC model, repopulation using feces derived from PDA-bearing KPC mice, but not WT mice, accelerated disease progression and mitigated the augmented T-cell infiltration associated with the germ-free condition (Supplementary Fig. S6B; Fig. 2B–D). Repopulation using *B. pseudolongum* similarly accelerated oncogenesis (Fig. 2B–D). Using FISH, we confirmed repopulation of the pancreas with *B. pseudolongum*, again indicating translocation of gut bacteria to the pancreas (Fig. 2E).

Figure 2. The microbiome in PDA-bearing hosts promotes tumor progression and intratumoral immune suppression. **A,** KC mice treated with an ablative oral antibiotic regimen (Abx) for 8 weeks were (i) repopulated with feces from 3-month-old WT mice, (ii) repopulated with feces from 3-month-old KPC mice, or (iii) sham-repopulated (vehicle only). Mice were sacrificed 8 weeks later, and pancreas weights from each cohort were compared with each other and to age-matched control KC mice that were not treated with antibiotics ($n = 3$–4/group). This experiment was repeated three times. **B–D,** The gut microbiome of germ-free (GF) 6-week-old KC mice were repopulated with feces from 3-month-old WT or KPC mice, *B. pseudolongum*, or sham-repopulated. Mice were sacrificed 8 weeks later. **B,** Tumor weights were measured. Each point represents data from a single mouse. **C,** Representative H&E-stained sections of pancreata are shown compared with age-matched non–germ-free controls (scale bar, 100 μm). Ductal histology was quantified. **D,** $CD3^+$ T-cell infiltration was determined by IHC. All repopulation experiments were repeated 3 times. HPF, high-power field. **E,** The gut microbiome of germ-free 6-week-old KC mice were repopulated with *B. pseudolongum* or sham-repopulated ($n = 5$/group). Colonization of pancreata with *B. pseudolongum* was confirmed using FISH at 8 weeks. This experiment was repeated twice. **F,** Control and oral antibiotic-treated WT mice were orthotopically implanted with KPC-derived tumor cells. $Gr1^-CD11b^+F4/80^+$ macrophages were gated and assessed for expression of CD206, MHC II, CD86, TNFα, IL12, IL6, and IL10 ($n = 5$/group). Macrophage profiling experiments were repeated more than 5 times. **G** and **H,** Splenic macrophages from untreated mice were harvested and cultured *in vitro* with cell-free extract from gut bacteria of control or KC mice. After 24 hours, macrophages were analyzed for expression of (**G**) MHC II and (**H**) IL10 ($n = 18$/group). **I,** Splenic macrophages were cultured *in vitro* with cell-free extract from *B. pseudolongum* or with PBS. After 24 hours, macrophages were analyzed for expression of TNFα. Macrophage polarization experiments were repeated 3 times in replicates of 5. **J–M,** Control and oral antibiotic-treated WT mice were orthotopically implanted with KPC-derived tumor cells. $CD4^+$ and $CD8^+$ T cells were gated and tested for expression of (**J**) T-BET, (**K**) TNFα, (**L**) PD-1, and (**M**) CD44. Representative contour plots and quantitative data are shown. Immune-phenotyping experiments were repeated more than 5 times ($n = 5$/group; *, $P < 0.05$; **, $P < 0.01$; ***, $P < 0.001$; ****, $P < 0.0001$).

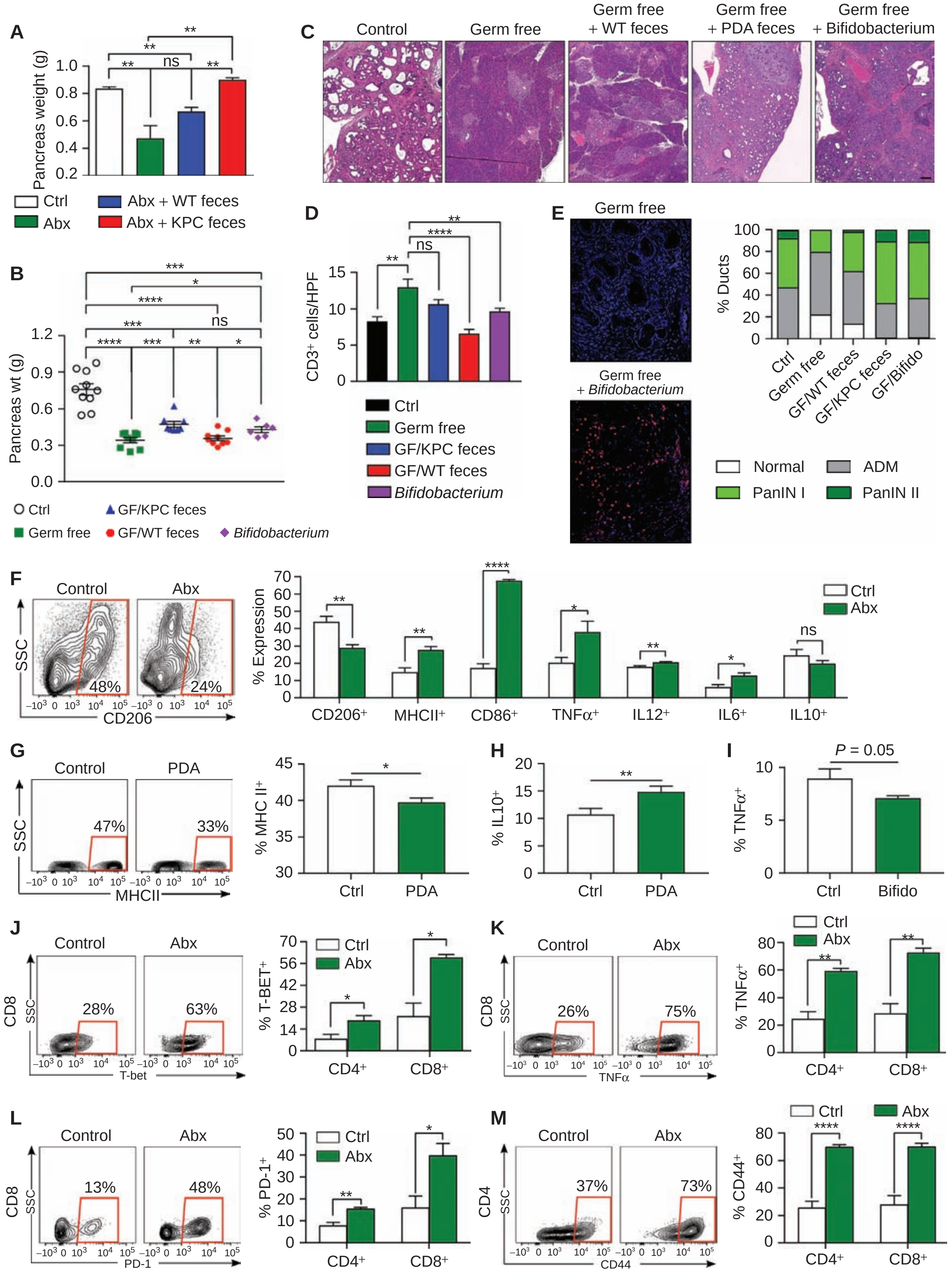
A
Pancreas weight (g)
1.0
0.8
0.6
0.4
0.2
** ** ** ns **
Ctrl
Abx
Abx + WT feces
Abx + KPC feces
B
Pancreas wt (g)
1.2
0.9
0.6
0.3
0.0
*** * **** *** ns **** *** ** *
Ctrl
Germ free
GF/KPC feces
GF/WT feces
Bifidobacterium
C
Control
Germ free
Germ free + WT feces
Germ free + PDA feces
Germ free + Bifidobacterium
D
CD3+ cells/HPF
15
10
5
0
** **** ns **
Ctrl
Germ free
GF/KPC feces
GF/WT feces
Bifidobacterium
E
Germ free
Germ free + Bifidobacterium
% Ducts
100
80
60
40
20
0
Ctrl
Germ free
GF/WT feces
GF/KPC feces
GF/Bifido
Normal
ADM
PanIN I
PanIN II
F
Control
Abx
SSC
48%
24%
CD206
% Expression
70
60
50
40
30
20
10
0
** ** **** * ** * ns
CD206+
MHCII+
CD86+
TNFα+
IL12+
IL6+
IL10+
Ctrl
Abx
G
Control
PDA
SSC
47%
33%
MHCII
% MHC II+
45
40
35
30
*
Ctrl
PDA
H
% IL10+
20
15
10
5
0
**
Ctrl
PDA
I
P = 0.05
% TNFα+
10
5
0
Ctrl
Bifido
J
Control
Abx
CD8 SSC
28%
63%
T-bet
% T-BET+
70
56
42
28
14
0
* *
Ctrl
Abx
CD4+
CD8+
K
Control
Abx
CD8 SSC
26%
75%
TNFα
% TNFα+
80
60
40
20
0
** **
Ctrl
Abx
CD4+
CD8+
L
Control
Abx
CD8 SSC
13%
48%
PD-1
% PD-1+
50
40
30
20
10
0
** *
Ctrl
Abx
CD4+
CD8+
M
Control
Abx
CD4 SSC
37%
73%
CD44
% CD44+
80
60
40
20
0
**** ****
Ctrl
Abx
CD4+
CD8+

We postulated that the microbiome promotes PDA progression by inducing peritumoral immune suppression. Consistent with our IHC results in the KC model, we found that microbial ablation resulted in a marked increase in the fraction of intratumoral T cells and a reduction in the fraction of myeloid-derived suppressor cells (MDSC) in the orthotopic KPC model (Supplementary Fig. S6C and S6D). Analysis of the phenotype of tumor-associated macrophages (TAM) suggested that microbial ablation leads to a reduction in immune-suppressive $CD206^+$ M2-like TAM with a concomitant increase in M1-like TAMs, expressing higher MHC II, CD86, TNFα, IL12, and IL6 (Fig. 2F). Analysis of chemokine expression suggested that TAMs infiltrating tumors of antibiotic-treated mice expressed increased levels of numerous M1-assoicated chemokines (Supplementary Fig. S6E). We found that cell-free extract from gut bacteria of PDA-bearing hosts reduced MHC II expression, but upregulated IL10, in splenic macrophages compared with cell-free extract from gut bacteria of control mice (Fig. 2G and H). Cell-free extract from *B. pseudolongum* had similar effects at mitigating M1 differentiation of macrophages (Fig. 2I). Because we reported that macrophage polarization dictates T-cell immunogenicity in PDA (6, 11), we postulated that bacterial ablation would activate the tumor-infiltrating T-cell population. Accordingly, antimicrobial treatment resulted in an increased intratumoral CD8:CD4 T-cell ratio (Supplementary Fig. S6F), which is associated with enhanced immunogenicity in PDA (12). Moreover, microbial ablation enhanced the TH1 polarization of $CD4^+$ T cells and the acquisition of a cytotoxic $CD8^+$ T-cell phenotype as evidenced by upregulation of T-BET (Fig. 2J), TNFα (Fig. 2K), IFNγ, and CD38 (Supplementary Fig. S6G and S6H). Both intratumoral $CD4^+$ and $CD8^+$ T cells in antibiotic-ablated mice also increased their expression of PD-1 (Fig. 2L) and CD44 (Fig. 2M), and $CD4^+$ T cells expressed higher ICOS and LFA1 (Supplementary Fig. S6I). Regulatory T cell (Treg) differentiation was not affected by bacterial ablation (Supplementary Fig. S6J). Antibiotic ablation also increased intratumoral immunogenicity in the orthotopic Pan02 model (Supplementary Fig. S6K–S6M). Notably, repopulation of the microbiome after antibiotic ablation using feces derived from KPC mice reversed the intratumoral immunogenic changes associated with bacterial ablation (Supplementary Fig. S6N–S6P). Whole pancreas NanoString array confirmed that genes associated with T-cell proliferation and immune activation were upregulated in tumors of antibiotic-treated mice (Supplementary Fig. S7A). Collectively, these data suggest that the microbiome regulates immunogenicity in PDA.

To further investigate whether microbiome-entrained macrophages mediate T-cell suppression in PDA, we stimulated $CD4^+$ and $CD8^+$ T cells using CD3/CD28 coligation either alone or in the presence of splenic macrophages that had been treated with cell-free extract from gut bacteria derived from WT mice or KC mice. Macrophages entrained by gut bacterial extracts from PDA-bearing hosts mitigated $CD4^+$ and $CD8^+$ T-cell activation, as evidenced by reduced expression of CD44 and PD-1, and prevented TH1 differentiation in $CD4^+$ T cells, as determined by expression of T-BET (Fig. 3A–E). By contrast, macrophages entrained by gut bacteria of control mice were largely noninhibitory. We further tested whether macrophages entrained by the PDA microbiome were deficient at antigen presentation. Consistent with our previous data, Ova-pulsed macrophages treated with cell-free extract from gut bacteria derived from PDA-bearing hosts exhibited a reduced capacity to activate and induce TH1 differentiation in Ova-restricted $CD4^+$ T cells (Fig. 3F–I). Similarly, TAMs harvested from PDA tumors in antibiotic-ablated mice exhibited increased capacity to activate T cells relative to TAMs from PDA tumors in control mice (Fig. 3J). Moreover, *in vivo* macrophage neutralization abrogated the intratumoral T-cell activation associated with microbial ablation in PDA (Fig. 3K–M).

To definitively implicate enhanced adaptive immunity in the tumor protection associated with microbial ablation, we harvested T cells from orthotopic KPC tumors in either control or antibiotic-treated mice and adoptively transferred the T cells to cohorts of mice challenged with subcutaneous KPC tumor. Transfer of PDA-infiltrating T cells from control mice failed to protect; however, tumor-infiltrating T cells derived from antibiotic-treated mice reduced tumor burden by ~50% (Fig. 3N). Accordingly, T-cell depletion abrogated the tumor-protective effects of bacterial ablation but did not affect the rate of tumor growth in PDA-bearing control mice (Fig. 3O). Furthermore, because bacterial

Figure 3. The PDA microbiome promotes macrophage-mediated suppression of T-cell immunity. **A–E,** Naïve splenic $CD4^+$ and $CD8^+$ T cells from WT mice were activated using CD3/CD28 coligation, either alone or in the presence of splenic macrophages that had been treated overnight with cell-free extract from gut bacteria derived from 3-month-old WT mice or KC mice. $CD4^+$ and $CD8^+$ T-cell activation, respectively, were determined by expression of (**A**, **B**) CD44 and (**C**, **D**) PD-1. **E,** $CD4^+$ T-cell differentiation was further evaluated by expression of T-BET. This experiment was repeated more than 5 times using 3–5 replicates per group. **F–I,** Splenic macrophages that had been treated overnight with cell-free extract from gut bacteria derived from 3-month-old WT mice or KC mice were pulsed with $Ova_{323\text{-}339}$ peptide and used to stimulate $CD4^+$ OT-II T cells. T-cell activation at 96 hours was determined by expression of (**F**) T-BET, (**G**) TNFα, (**H**) CD44, and (**I**) LFA1. This experiment was repeated 4 times using 4–5 replicates per group. **J,** Control and oral antibiotic-treated (Abx) WT mice bearing orthotopic KPC-derived tumor cells were sacrificed at 21 days. TAMs were FACS-sorted, loaded with $Ova_{257\text{-}264}$ peptide and used to stimulate Ova-restricted $CD8^+$ OT-I T cells. T-cell activation was determined by expression of TNFα, IFNγ, CD69, and PD-1. This experiment was repeated 3 times ($n = 5$/group). **K–M,** Cohorts of orthotopic PDA-bearing mice treated with oral PBS or ablative antibiotics were serially administered neutralizing αF480 or isotype control ($n = 10$/group). Mice were sacrificed at 21 days and tumor-infiltrating T cells were analyzed for (**K**) the CD8:CD4 ratio, (**L**) $CD4^+$ T-cell expression of CD44, LFA1, IFNγ, and T-BET, and (**M**) $CD8^+$ T-cell expression of LFA1 and T-BET. **N,** PDA-infiltrating T cells from orthotopic KPC tumor–bearing mice that had been treated with an ablative oral antibiotic regimen or sham-treated were harvested on day 21 by FACS, mixed with FC1242 cells in a 1:10 ratio, and subcutaneously implanted in the flank of recipient mice. Additional controls received FC1242 cells alone. Tumor volumes were measured at serial intervals. This experiment was repeated 3 times ($n = 4$/group). **O,** Cohorts of orthotopic PDA-bearing mice treated with oral PBS or ablative antibiotics were serially administered neutralizing αCD4 and αCD8 mAbs or isotype control. Mice were sacrificed at 21 days and pancreatic tumors were weighed ($n = 8$–9/group). T-cell depletion experiments were performed more than 3 times in orthotopic PDA-bearing mice. **P,** WT mice were treated with vehicle ($n = 9$), αPD-1 ($n = 16$), an ablative oral antibiotic regimen ($n = 6$), or both ($n = 9$). Mice were challenged with orthotopic KPC tumor and sacrificed at 3 weeks. Treatments were started before tumor implantation and continued until the time of sacrifice. This experiment was repeated 4 times ($n = 10$/group; *, $P < 0.05$; **, $P < 0.01$; ***, $P < 0.001$; ****, $P < 0.0001$).

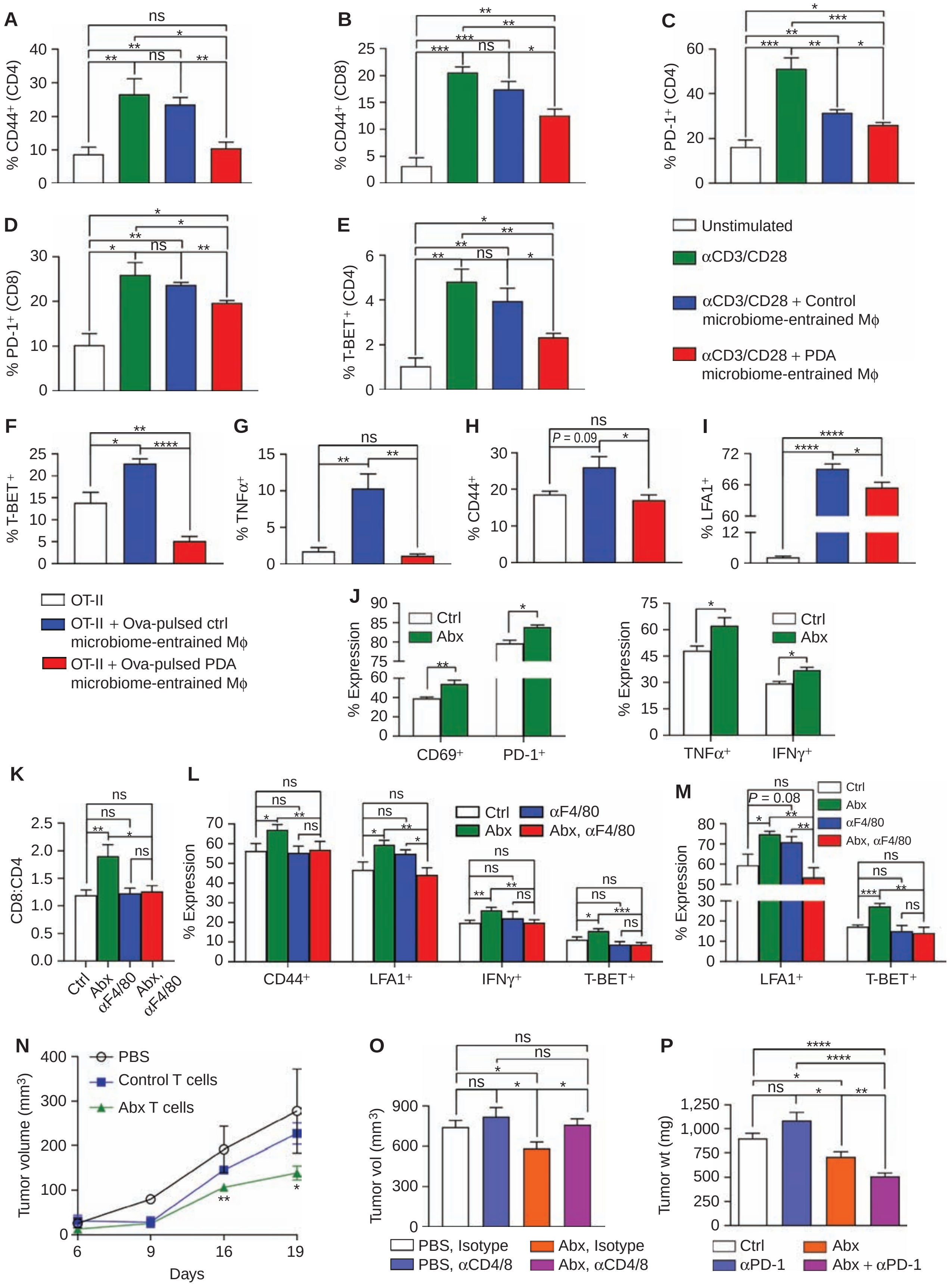
A
% CD44+ (CD4)
0
10
20
30
40
ns
*
**
**
ns
**
B
% CD44+ (CD8)
0
5
10
15
20
25
**
**
***
***
ns
*
C
% PD-1+ (CD4)
0
20
40
60
*
***
**
***
**
*
D
% PD-1+ (CD8)
0
10
20
30
*
*
**
*
ns
**
E
% T-BET+ (CD4)
0
2
4
6
*
**
**
**
ns
*
Unstimulated
αCD3/CD28
αCD3/CD28 + Control microbiome-entrained Mϕ
αCD3/CD28 + PDA microbiome-entrained Mϕ
F
% T-BET+
0
5
10
15
20
25
**
*
****
G
% TNFα+
0
5
10
15
ns
**
**
H
% CD44+
0
10
20
30
ns
P = 0.09
*
I
% LFA1+
0
12
60
66
72
****
****
*
OT-II
OT-II + Ova-pulsed ctrl microbiome-entrained Mϕ
OT-II + Ova-pulsed PDA microbiome-entrained Mϕ
J
% Expression
0
20
40
60
75
80
85
90
Ctrl
Abx
**
*
CD69+
PD-1+
% Expression
0
15
30
45
60
75
*
*
Ctrl
Abx
TNFα+
IFNγ+
K
CD8:CD4
0.0
0.5
1.0
1.5
2.0
2.5
ns
ns
**
*
ns
Ctrl
Abx
αF4/80
Abx, αF4/80
L
% Expression
0
10
20
30
40
50
60
70
ns
ns
*
**
ns
ns
ns
*
**
*
Ctrl
Abx
αF4/80
Abx, αF4/80
ns
ns
**
**
ns
ns
ns
*
***
ns
CD44+
LFA1+
IFNγ+
T-BET+
M
% Expression
0
10
20
30
50
60
70
80
ns
P = 0.08
*
**
**
Ctrl
Abx
αF4/80
Abx, αF4/80
ns
ns
***
**
ns
LFA1+
T-BET+
N
Tumor volume (mm3)
0
100
200
300
400
PBS
Control T cells
Abx T cells
**
*
6
9
16
19
Days
O
Tumor vol (mm3)
0
300
600
900
ns
ns
*
ns
*
*
PBS, Isotype
PBS, αCD4/8
Abx, Isotype
Abx, αCD4/8
P
Tumor wt (mg)
0
250
500
750
1,000
1,250
****
****
*
ns
*
**
Ctrl
αPD-1
Abx
Abx + αPD-1

ablation upregulated PD-1 expression in intratumoral CD4$^+$ and CD8$^+$ T cells (Fig. 2L), we postulated that microbial ablation would have synergistic efficacy with PD-1–directed therapies. Whereas PD-1 blockade did not protect control mice against orthotopic PDA, ablative oral antibiotics coupled with αPD-1 therapy was synergistically protective based on tumor size (Fig. 3P). Combined antibiotic + αPD-1 therapy also resulted in enhanced intratumoral CD4$^+$ and CD8$^+$ T-cell activation (Supplementary Fig. S7B and S7C). In addition, T cells upregulated CXCR3 and LFA1, which were not increased in expression with either monotherapy alone (Supplementary Fig. S7D and S7E).

We previously reported that diverse PRRs, including TLR3, TLR4, TLR7, TLR9, NLRP3, Dectin-1, and Mincle, are upregulated in PDA and their activation accelerates oncogenesis via induction of innate and adaptive immune suppression (2–4, 13, 14). We postulated that the immune tolerance promoted by the PDA microbiome is the result of higher PRR activation in the tumor microenvironment. Consistent with our hypothesis, we found that cell-free extract from gut bacteria derived from KC mice induced higher activation of diverse PRR reporter cell lines, most notably TLR2, TLR4, and TLR5, compared with gut bacterial extract from WT mice (Fig. 4A). Further, PDA tumors in antibiotic-ablated hosts exhibited markedly lower expression of PRRs and associated signaling molecules compared with PDA tumors in control mice (Fig. 4B). We confirmed that, similar to the PRRs we previously studied, expression of TLR2 and TLR5 was upregulated in macrophages in PDA by flow cytometry (Fig. 4C and D), and their ligation accelerated tumor growth (Fig. 4E and F) and accentuated innate and adaptive immune suppression (Fig. 4G–M). Moreover, *in vivo* inhibition of TLR signaling by blocking TRAF6 abrogated the PDA-promoting effects of repopulating antibiotic-ablated mice with KPC feces or *B. pseudolongum* (Fig. 4N). Further, macrophages entrained by the PDA microbiome in the context of inhibition of TLR signaling failed to suppress T-cell immunogenicity, suggesting that the PDA microbiome programs TAMs via TLR signaling to induce immune tolerance (Fig. 4O–R).

A primary uncertainty in tumor biology is the question of why oncogenesis proceeds at variable rates in hosts with similar genetic risk factors. A quintessential example of this in murine modeling of cancer is the variable tumor phenotype in KPC mice (15). We postulated that a factor driving phenotypic variance in PDA progression in genetically identical mice is the degree of bacterial dysbiosis. To address this, we prospectively collected fecal specimens from 12-week-old KPC mice, segregated them into aggressive PDA (adv-KPC) and slowly progressive (ea-KPC) disease groups based on microscopic disease progression (Supplementary Fig. S8A), and compared their gut microbial phenotypes to age-matched littermate WT controls. *Bacteroides* and *Lactobacillus* were among the most predominant genera in the three cohorts (Supplementary Fig. S8B). LDA analysis revealed that, similar to data in the KC model, numerous genera belonging to *Bacteroidetes* and *Firmicutes* and select *Actinobacteria*- and *Deferribacteres*-associated genera were more prevalent in the ea-KPC and adv-KPC cohorts compared with WT (Supplementary Fig. S8C and S8D). When we contrasted the microbial genera in ea-KPC and adv-KPC mice, we observed that *Elizabethkingia, Enterobacteriaceae*, and *Mycoplasmataceae* were significantly overrepresented in ea-KPC, whereas *Helicobacteraceae, Bacteroidales*, and *Mogibacteriaceae* were more prevalent in adv-KPC (Supplementary Fig. S8E). Global relationships between microbial communities of the WT, ea-KPC, and adv-KPC cohorts were analyzed by PCoA, indicating significant variations between the cohorts and a high degree of similarity within each individual cohort (Supplementary Fig. S8F). Accordingly, fecal phylogenetic diversity was significantly different among the 3 murine subsets (Supplementary Fig. S8G). LDA analysis of the human PDA gut microbiome similarly indicated significant differences in bacterial abundances between stage I/II and stage IV patients (Supplementary Fig. S8H). Collectively, these data suggest that bacterial communities are distinct between early and advanced PDA.

DISCUSSION

The gut microbiome is known to be important in the maintenance of homeostasis in several physiologic processes, including host energy metabolism, gut epithelial permeability, gut peptide hormone secretion, and host inflammatory state. Microbial dysbiosis is also being increasingly recognized for its role in oncogenesis (16, 17). We found that germ-free mice are protected against PDA progression. Oral antibiotic administration also slowed oncogenic progression, whereas select bacterial transfer or bulk fecal transfer from PDA-bearing mice, but not control mice, accelerated tumorigenesis. These

Figure 4. The PDA microbiome induces immune suppression via differential TLR activation. **A,** Cell-free extract from gut bacteria derived from 3-month-old WT or KC mice ($n = 3$) were tested for activation of a diverse array of PRR-specific HEK293 reporter cell lines. **B,** Orthotopic KPC tumors were harvested on day 21 from control and oral antibiotic–treated WT mice. PRR-related gene expression in PDA was determined using a PCR array and performed in duplicate. Data indicate fold change in gene expression for control compared with antibiotic-treated groups. This array was repeated twice. **C,** Expression of TLR2 and **D,** TLR5 were tested in spleen and PDA-infiltrating macrophages from orthotopic KPC tumors ($n = 5$). These experiments were repeated twice. **E,** WT mice were orthotopically implanted with KPC-derived tumor cells and serially treated with TLR2 (Pam_3CSK_4) or (**F**) TLR5 (Flagellin) ligand or vehicle. Tumor growth was determined at 3 weeks ($n = 3$–5/group). These experiments were repeated twice. **G–K,** WT mice were orthotopically implanted with KPC-derived tumor cells and serially treated with TLR5 ligand. Tumors were harvested at 3 weeks and (**G**) the fraction of Gr1$^+$CD11b$^+$ MDSC and (**H**) F4/80$^+$Gr1$^-$CD11b$^+$ TAM infiltration was determined by flow cytometry. **I,** Expression of MHC II, TNFα, and CD38 on TAMs was determined. **J,** The CD8/CD4 T-cell ratio was determined as was (**K**) TNFα expression on CD4$^+$ and CD8$^+$ T cells ($n = 3$–5/group). **L** and **M,** WT mice were orthotopically implanted with KPC-derived tumor cells and serially treated with TLR2 ligand. Tumors were harvested at 3 weeks, and (**L**) the CD8/CD4 T-cell ratio and (**M**) TAMs expression of TNFα were determined. These experiments were repeated twice ($n = 3$–5/group). **N,** WT mice pretreated with an ablative oral antibiotic regimen or vehicle for 6 weeks were (i) repopulated with feces from 3-month-old KPC mice ($n = 12$), (ii) repopulated with *B. pseudolongum* ($n = 6$), or (iii) sham-repopulated ($n = 4$). Mice were challenged with orthotopic KPC cells. Cohorts were additionally treated serially with a TRAF6 inhibitor or control. Treatments were started at the time of tumor implantation and continued until sacrifice at 21 days. Quantitative analysis of tumor weights is shown. **O–R,** Splenic macrophages were entrained with extract from the gut microbiome of either WT or KC mice in the context of MyD88 inhibition or control. Macrophages were then used in αCD3/αCD28-based T-cell stimulation assays. CD4$^+$ T-cell activation was determined by expression of (**O**) LFA1, (**P**) CD44, (**Q**) TNFα, and (**R**) IFNγ. This experiment was repeated 5 times in 3–4 replicates per group with similar results (*, $P < 0.05$; **, $P < 0.01$; ***, $P < 0.001$; ****, $P < 0.0001$).

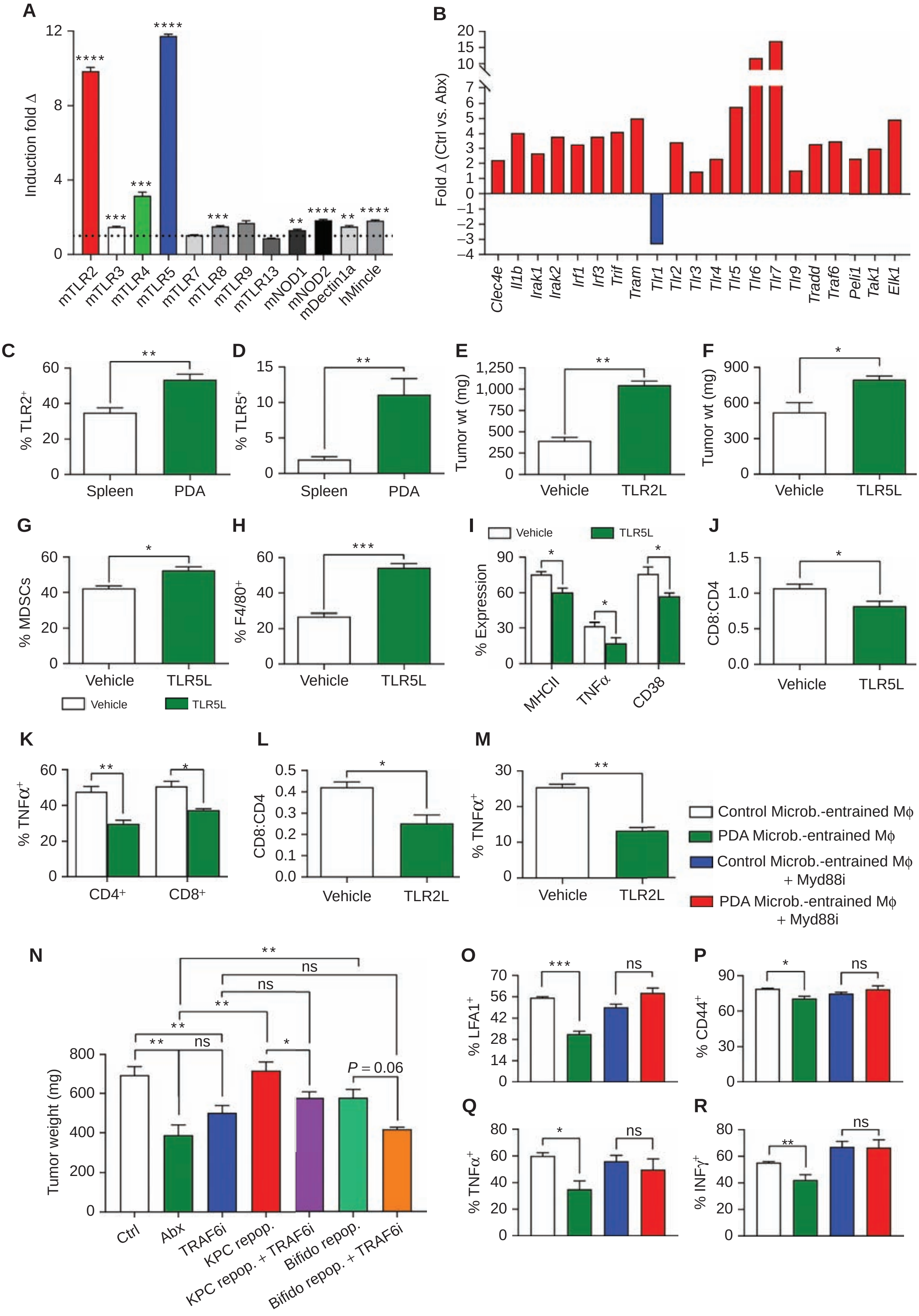
A
Induction fold Δ
0
4
8
12
****
***
***
****
***
**
****
**
****
mTLR2
mTLR3
mTLR4
mTLR5
mTLR7
mTLR8
mTLR9
mTLR13
mNOD1
mNOD2
mDectin1a
hMincle
B
Fold Δ (Ctrl vs. Abx)
20
15
10
7
6
5
4
3
2
1
0
−1
−2
−3
−4
Clec4e
Il1b
Irak1
Irak2
Irf1
Irf3
Trif
Tram
Tlr1
Tlr2
Tlr3
Tlr4
Tlr5
Tlr6
Tlr7
Tlr9
Tradd
Traf6
Peli1
Tak1
Elk1
C
% TLR2+
**
Spleen
PDA
D
% TLR5+
**
Spleen
PDA
E
Tumor wt (mg)
1,250
1,000
750
500
250
0
**
Vehicle
TLR2L
F
Tumor wt (mg)
900
600
300
0
*
Vehicle
TLR5L
G
% MDSCs
*
Vehicle
TLR5L
H
% F4/80+
***
Vehicle
TLR5L
I
Vehicle
TLR5L
% Expression
90
60
30
0
*
*
*
MHCII
TNFα
CD38
J
CD8:CD4
1.5
1.0
0.5
0.0
*
Vehicle
TLR5L
Vehicle
TLR5L
K
% TNFα+
**
*
CD4+
CD8+
L
CD8:CD4
0.5
0.4
0.3
0.2
0.1
0.0
*
Vehicle
TLR2L
M
% TNFα+
30
20
10
0
**
Vehicle
TLR2L
Control Microb.-entrained Mϕ
PDA Microb.-entrained Mϕ
Control Microb.-entrained Mϕ + Myd88i
PDA Microb.-entrained Mϕ + Myd88i
N
Tumor weight (mg)
800
600
400
200
0
**
ns
ns
**
**
**
ns
*
P = 0.06
Ctrl
Abx
TRAF6i
KPC repop.
KPC repop. + TRAF6i
Bifido repop.
Bifido repop. + TRAF6i
O
% LFA1+
70
56
42
28
14
0
***
ns
P
% CD44+
90
60
30
0
*
ns
Q
% TNFα+
80
60
40
20
0
*
ns
R
% INFγ+
80
60
40
20
0
**
ns

observations support a role for the microbiome in promoting disease progression. However, it is also likely that oncogenic *Kras* expression influences the composition and diversity of the gut and intrapancreatic flora. Moreover, our data suggest oral antibiotics may be useful as a chemopreventive measure for high-risk patients with advanced PanIN lesions or for individuals at increased genetic risk for PDA development. This also raises the prospect of a potential role for probiotics in mitigating PDA risk.

Inflammation is paramount for PDA development and progression. PDA is invariably preceded by and associated with a robust inflammatory cell infiltrate that has profound influences on disease progression (18). Specific intrapancreatic leukocytic subsets can have divergent effects on tumorigenesis either by combating cancer growth via innate or antigen-restricted tumoricidal immune responses or by promoting tumor progression by inducing immune suppression (19). TH1 $CD4^+$ T cells and $CD8^+$ T cells mediate tumor protection in murine models of PDA and are associated with prolonged survival in human disease (20). Conversely, we recently reported that antigen-restricted TH2-deviated $CD4^+$ T cells promote pancreatic tumor progression in mice (4). Accordingly, intratumoral $CD4^+$ TH2 cell infiltrates correlate with reduced survival in human PDA (20, 21). $FOXP3^+$ Tregs also facilitate tumor immune escape in PDA (22). However, regulation of the balance between immunogenic and immune-suppressive myeloid and subsequent T-cell differentiation in PDA is uncertain. We discovered that the microbiome is a potent modulator of the programming of the inflammatory tumor microenvironment.

We demonstrated that the distinct bacterial dysbiosis associated with PDA results in both innate and adaptive immune suppression. Depletion of the gut microbiome led to a diminution of MDSC infiltration and reprogramming of TAM toward a tumor-protective M1-like phenotype. We recently reported that macrophage polarization dictates effector T-cell phenotype in PDA (6). Accordingly, ablation of the gut microbiome accentuated TH1 polarization of $CD4^+$ T cells and enhanced the cytotoxic phenotype of $CD8^+$ T cells, as evidenced by high T-BET, TNFα, and IFNγ expression. Our findings that gut bacterial ablation induces immunogenic reprogramming of the tumor microenvironment and markedly increases PD-1 expression on effector T cells suggest that oral antibiotics in combination with checkpoint-directed immunotherapy may be an attractive strategy for experimental therapeutics in patients with PDA. Targeting the microbiome has also been recently shown to synergize with cytotoxic chemotherapy in select cancers by affecting the metabolism of the chemotherapeutic agents (23).

The etiologic relationship between gut bacteria and immune-suppressive inflammation in PDA has not been previously described. Recent work by our group and others has shown that ligation of select PRRs accelerates PDA progression, whereas their inhibition or genetic deletion is protective (2–6, 17, 18). Here, we demonstrate that TLR2 and TLR5 ligation promotes PDA and induces innate and adaptive immune suppression. Moreover, we found that the immune-suppressive effects of PDA-associated bacterial extract on macrophages were absent in macrophages deficient in TLR signaling, suggesting that the suppressive effects of the PDA microbiome on macrophage programming are dependent on TLR ligation. Specifically, we show that the suppressive effects of PDA-microbiome entrained macrophages on T-cell activation are abrogated in the absence of TLR signaling. Moreover, although repopulation of antibiotic-ablated mice with the KPC microbiome or with *B. pseudolongum* accelerated oncogenesis, this tumor-promoting effect was abated when TLR signaling was abrogated *in vivo*. Collectively, these data show mechanistic evidence that tumor-promoting effects of the PDA microbiome are TLR dependent.

To improve upon the potential for biomarker discovery or development of novel therapies, it is imperative to elucidate the specific microbial taxa associated with organ-specific oncogenesis. Our bacterial translocation experiments suggest interactions between the two compartments, presumably via the pancreatic duct which is in anatomic continuity with the intestinal tract. In human adults, *Bacteroidetes* and *Firmicutes* usually dominate the intestinal microbiota, whereas *Actinobacteria, Proteobacteria*, and *Verrucomicrobia* represent a minor proportion (24). Conversely, *Proteobacteria, Actinobacteria, Fusobacteria*, and *Verrucomicrobia* were each higher in the gut of patients with PDA as compared with healthy controls. Interestingly, *Proteobacteria* was also enriched in the intrapancreatic microbiome in PDA-bearing patients and was associated with advanced disease. The increased translocation of this pathogenic gram-negative taxa supports the observation that ligation of select TLRs by lipopolysaccharides and flagellins can promote tolerogenic macrophage programming in the tumor microenvironment.

A group of pathogens, even at low abundance within the microbial community, can act as keystone species or signatures that support and shape community structure and membership in a manner that promotes disease pathogenesis (25). The skewed microbial structure and membership in human gut and pancreatic tissues of patients with PDA and in mouse models of pancreatic cancer reiterate the possible involvement of monobacterial or polybacterial communities in the initiation and progression of PDA. We found that *B. pseudolongum* was differentially abundant in gut and tumor and accelerated oncogenesis in a TLR-dependent manner. In addition, cell-free extracts from *B. pseudolongum* polarized macrophages to upregulate tolerogenic cytokines including IL10. Recent studies similarly reported a higher abundance of *Bifidobacterium* in the tissues of patients with colorectal adenomas (26, 27). By contrast, a recent report showed that commensal *B. longum* conferred protection in melanoma by promoting anti–PD-L1 therapy, indicating that different species may have diverging effects in the tumor microenvironment (28).

In summary, our study elucidates the presence of a distinct gut microbiome that is associated with progressive pancreatic oncogenesis in mice. We show that the pancreas harbors its own microbiome that is associated with disease stage in mice and humans. We also detail the intrapancreatic immune programming induced by the microbiome. Modulation of the PDA microbiome to augment immunotherapy is an attractive avenue for experimental therapeutics. Further, prospective studies are necessary for identification of microbial signatures with tumor specificity that may have potential for early diagnosis and risk stratification.

METHODS

Animals and In Vivo *Models*

KC mice, which develop spontaneous pancreatic neoplasia by targeted expression of mutant *Kras* in the pancreas, were a gift from Dafna Bar-Sagi (New York University; ref. 29). C57BL/6 (H-2Kb) mice (WT) were originally purchased from The Jackson Laboratory and were bred in-house and crossed with the KC model after 8 generations. Littermate controls were used in experiments. Animals were housed in a specific pathogen-free vivarium and fed standard mouse chow. KPC mice, which express mutant intrapancreatic *Kras* and *Trp53*, were a gift from Mark Phillips (New York University; ref. 15). OT-I and OT-II mice were purchased from The Jackson Laboratory and bred in-house. Both male and female mice were used, but animals were sex- and age-matched in each experiment. For orthotopic tumor experiments, 8- to 10-week-old mice were used. No formal power analyses, randomization, exclusions, or blinding were performed. Mice were administered intrapancreatic injections of tumor cells derived from pancreata of KPC mice (10^5 cells in Matrigel; generated from KPC mice as described in ref. 2; utilized within 6 months of generation; not reauthenticated during this time) and were sacrificed after 3 weeks, as previously described (2). Alternatively, mice were administered intrapancreatic injections of Pan02 tumor cells (10^6 cells in Matrigel; gift of and authenticated by Daniel Meruelo, New York University, received May 2016) and sacrificed at 5 weeks. Both cell lines were commercially MAP tested by Taconic in December 2016 via RAPIDMAP-12 panel and all results were negative. In select experiments, mice were serially treated with a neutralizing αPD-1 mAb (150 μg, i.p., RMP1-14, 2×/week; Bioxcell). In other experiments, CD4$^+$ T cells (GK1.5), CD8$^+$ T cells (53-6.72), or F480$^+$ macrophages (CI:A3-1; all BioXCell) were depleted with neutralizing mAbs using regimens as previously described (6, 30). Alternatively, mice were serially treated with TRAF6 inhibitor (66 μg, i.p., 3×/week; Novus Biologicals), TLR2 (Pam$_3$CSK$_4$, 50 μg, i.p., 3×/week) or TLR5 (Flagellin, 10 μg, i.p., 2×/week; both Invivogen) ligands. For T-cell transfer experiments, intratumoral T cells were harvested by FACS, mixed with 10^5 FC1242 cells in a 1:10 ratio, and subcutaneously implanted into the flank of recipient mice. Germ-free KC mice were generated by rederiving and crossing *Ptf1a*$^{\text{Cre}}$ and LSL-*Kras*$^{\text{G12D}}$ mice in a germ-free environment at the National Gnotobiotic Rodent Resource Center (Chapel Hill, NC). Longitudinal cohort studies were conducted to monitor microbial communities throughout experiments by serially collecting specimens from littermate WT and KC or KPC mice. Fecal and tissue specimens were stored in sterile tubes at −80°C until further use.

Antibiotic Treatment, Fecal, and Bacterial Transfer Experiments

To ablate the gut microbiome, 6-week-old WT or KC mice were administered an antibiotic cocktail by oral gavage daily for five consecutive days. Controls were gavaged with PBS. The oral gavage cocktail contained vancomycin (50 mg/mL; Sigma), neomycin (10 mg/mL; Sigma), metronidazole (100 mg/mL; Santa Cruz Biotech), and amphotericin (1 mg/mL; MP Biomedicals), as described (31). Additionally, for the duration of the experiments, mouse drinking water was mixed with ampicillin (1 mg/mL; Santa Cruz Biotech), vancomycin (0.5 mg/mL; Sigma), neomycin (0.5 mg/mL; Sigma), metronidazole (1 mg/mL; Santa Cruz Biotech), and amphotericin (0.5 μg/mL; MP Biomedicals). In fecal transfer experiments, six fecal pellets from mice were collected and resuspended in 1 mL of PBS, and 200 μL of the fecal slurry was used for orogastric gavage every other day for 2 weeks. For species-specific repopulation experiments, *Bifidobacterium pseudolongum* [1×10^8 colony forming units (CFU)/mL; Cat. #25526, ATCC] was used to orally gavage germ-free mice at 6 weeks of age. Repopulation was confirmed by gram stain and qPCR of fecal sample and by FISH in pancreatic tissues. To assess bacterial translocation to the pancreas, WT mice were orally gavaged with 2.5×10^8 CFUs of *Enterococcus faecalis* that were labeled with CFSE according to the manufacturer's instructions (Invitrogen). Recipient mice were then serially sacrificed at 3-hour intervals, and their pancreata were harvested. Single-cell suspensions of pancreata were prepared and analyzed by flow cytometry for the presence of CFSE-labeled bacteria. Alternatively, GFP-labeled *Escherichia coli* (2.5×10^8 CFU) were introduced via oral gavage in mice, and pancreatic sections were examined at 3 hours by immune fluorescence microscopy. All experiments were approved by the New York University School of Medicine Institutional Animal Care and Use Committee.

Murine Cellular Isolation, Flow Cytometry, and In Vitro *Experiments*

Pancreatic leukocytes were harvested from mouse PDA as described previously (6). Briefly, pancreata were resected and placed in ice-cold PBS with 1% FBS, collagenase IV (1 mg/mL; Worthington Biochemical), and DNAse I (2 U/mL; Promega). After mincing, tissues were incubated in the same solution at 37°C for 20 minutes with gentle shaking. Specimens were then passed through a 70-μm mesh and centrifuged at 350× *g* for 5 minutes. Cells were resuspended in ice-cold PBS with 1% FBS. After blocking FcγRIII/II with an anti-CD16/CD32 mAb (eBioscience), cell labeling was performed by incubating 10^6 cells with 1 μg of fluorescently conjugated antibody directed against murine CD44 (IM7), CD206 (C068C2), PD-1 (29F.1A12), CD3 (17A2), CD4 (RM4-5), CD8 (53-6.7), CD45 (30-F11), CD11b (M1/70), Gr1 (RB6-8C5), CD11c (N418), CD38 (90), CD86 (GL-1), MHC II (M5/114.15.2), IL6 (MP5-20F3), IL10 (JES5-16E3), IL12/IL23 p40 (C15.6), IFNγ (XMG1.2), LFA1 (H155-78), CXCR3 (CXCR3-173), TNFα (MP6-XT22), TLR2 (6C2), TLR5 (ACT5), ICOS (15F9; all BioLegend), T-BET (4B10), and FOXP3 (FJK-16s; both eBioscience). Cell preparation for intracellular staining was performed using the Fixation and Permeabilization Solution Kit (eBiosciences). Flow cytometry was performed on the LSR-II (BD Biosciences). FACS sorting was performed on the SY3200 (Sony). Data were analyzed using FlowJo (TreeStar). Gates were based on isotype control. In select experiments, cell-free extract from 4×10^{12} CFU/mL bacteria from the gut of WT or KC (10-week-old) mice or *Bifidobacterium pseudolongum* (ATCC) was used for treatment of splenic macrophages overnight before analysis of macrophage phenotype by flow cytometry. In some experiments, MyD88-inhibitory peptide (200 μmol/L, Novus Biologicals) or control were added, as we described (4). Bacterial cell-free extracts were also used to activate HEK293 PRR reporter cell lines (Invivogen), as we previously described (13). For T-cell activation assays, splenic T cells were stimulated using plate-bound αCD3/αCD28 alone or in coculture with macrophages (5:1 ratio), as we described (13). Alternatively, antigen-restricted splenic CD4$^+$ OT-II T cells or CD8$^+$ OT-I T cells were stimulated using antigen-presenting cells pulsed with the appropriate Ova peptide, as we reported (32). T-cell activation was determined at 96 hours by flow cytometry. In select experiments, TAMs were cultured overnight at a concentration of 10^6 cells/mL before harvest of cell culture supernatant. Chemokine levels in cell culture supernatant were analyzed using the LEGENDplex bead array (BioLegend).

Histology, Immunohistochemistry, and RNA Analysis

For histologic analysis, pancreatic specimens were fixed with 10% buffered formalin, dehydrated in ethanol, embedded with paraffin, and stained with hematoxylin and eosin (H&E) and Gomori's Trichrome, anti-Ki67 (ab15580), anti-CD3 (ab5690, both Abcam), and TUNEL (Promega). The fraction of preserved acinar area was calculated as previously described (11). Histologic data from control KC mice were previously reported (6). The fraction and number of ducts containing all grades of PanIN lesions were measured by examining 10 high-power fields (40×) per slide. PanINs were graded according to established criteria (33): In PanIN I ducts, the normal cuboidal pancreatic epithelial cells transition to columnar architecture (PanIN Ia) and gain polyploid morphology (PanIN Ib). PanIN II lesions are associated with loss of polarity. PanIN III lesions, or *in situ* carcinoma, show cribriforming, budding off of cells, and luminal necrosis with marked cytologic abnormalities, without invasion beyond the basement membrane. Pancreata from 12-week-old KPC mice were segregated based on microscopic assessment by H&E staining of the percentage of pancreatic area occupied by invasive cancer: ea-KPC designated tumors exhibited <25% of pancreatic area occupied by invasive cancer; adv-KPC tumors exhibited >75% pancreatic area replacement by invasive cancer. Pancreata of mice with 25% to 75% invasive PDA were excluded from analysis so as to maintain distinctness of the groups. RNA extraction from pancreatic tumors was performed using the RNeasy Mini Kit (Qiagen) as per the manufacturer's instructions. For NanoString analysis, the nCounter mouse inflammation panel was used utilizing the nCounter Analysis System (both NanoString; ref. 34). In selected experiments, the preconfigured "Mouse TLR Signaling Pathway RT^2 Profiler PCR Array" was used as per the manufacturer's instructions (Qiagen).

Quantitative PCR

Total bacterial DNA in the pancreatic tissue and fecal samples was determined by real-time qPCR using 16S primers. Briefly, the 10 μL reaction mix contained 2× Power SYBR Green master mix (Applied Biosystems), 100 nmol/L of forward and reverse primers, and 15 ng sample DNA on the Bio-Rad CFX384 real-time system. The reaction was programmed as follows: denaturation at 94°C for 10 minutes, 40 cycles of 94°C for 1 minute, annealing at 60°C for 1 minute, and elongation at 72°C for 90 seconds, followed by a final elongation at 72°C for 5 minutes. *E. coli* DNA was used to plot a standard curve to calculate bacterial DNA concentration in the sample. A previously described standard protocol was used to convert CT values of each sample to total bacterial DNA in the sample (35).

FISH

The EUB338 16S rRNA gene probe or a *Bifidobacterium* specific probe labeled with the fluorophore Cy3 (extinction wavelength, 555 nm; emission wavelength, 570 nm; Molecular Probes) was used to detect the bacterial colonization within human and mouse pancreatic tissues by FISH. Fluorescence microscopic analysis was conducted with Nikon Eclipse 90i confocal microscope (Nikon) using a Cy3-labeled probe at 50 pmol/mL as described (36–38).

Human Sample Collection

Human fecal samples were collected from healthy volunteers and patients with PDA using rectal swabs. Specimens were stored in sterile TE buffer for 16S sequencing analysis. Patients who had been on antibiotic treatment within the past 3 months or patients who had received neoadjuvant chemotherapy or radiotherapy were excluded. Human tissue samples were sterilely collected from patients at NYU Langone Medical Center. Human specimens were obtained using an Institutional Review Board–approved protocol, conducted in accordance with the Declaration of Helsinki, the Belmont Report, and U.S. Common Rule, and donors of deidentified specimens gave written informed consent. All specimens were stored at −80°C till further use. Sample sizes for human experiments were not determined based on formal power calculations.

Bacterial DNA Extraction and Sequencing

Pancreatic tissue samples were suspended in 500 μL sterile PBS. Samples were pretreated by vortexing for 30 seconds followed by sonication and overnight treatment with Proteinase K (2.5 μg/mL) at 55°C, as we described previously (39, 40). Total bacterial genomic DNA was purified from tissue and fecal samples using the MoBio Power fecal kit as per the manufacturer's instructions (MoBio Laboratories Inc.). DNA was quantified for concentration and purity by NanoDrop 2000 spectrophotometer (Thermo Scientific) and stored at −20°C till further analysis. For high-throughput 16S rRNA library preparation and sequencing, the V3–V4 hypervariable region of the 16S gene was amplified from the genomic DNA of mice and human fecal and pancreatic tissue samples according to the Illumina 16S metagenomics protocol (Part #15044223 Rev. B; ref. 41). The purified DNA was quantified fluorometrically by the Quant-iT PicoGreen assay (Molecular Probes, Inc.) in a SpectraMax M5 microplate reader (Molecular Devices), and the concentration adjusted to 10 ng/μL for all sequencing assays. PCR was initially performed using the primer set 341F (5′-CCTACGGGNGGCWGCAG-3′) and 805R (5′-GACTACHVGGGTATCTAATCC-3′; refs. 41, 42), each with overhang adapter sequences (IDT) using 2× Kapa HiFi Hotstart ReadyMix DNA polymerase (KapaBiosystems). Samples were amplified in duplicate and purified using AMPure XP beads. Amplification was performed at 95°C (3 minutes), with 25 cycles of 95°C (30 seconds), 55°C (30 seconds), 72°C (30 seconds), and final extension of 72°C (5 minutes). Dual indices from Illumina Nextera XT index kits (Illumina) were added to target amplicons in a second PCR using 2× Kapa HiFi Hotstart ReadyMix DNA polymerase. PCR conditions were 95°C (3 minutes), with 8 cycles of 95°C (30 seconds), 55°C (30 seconds), 72°C (30 seconds), and final extension of 72°C (5 minutes). After each PCR cycle, AMPure XP bead–purified libraries were checked for purity by nanodrop, quantified by PicoGreen assay, and size confirmed on agarose gels. Negative controls were included in all sequencing runs. Equimolar amounts of the generated libraries with dual index were combined and quantified fluorometrically. The pooled amplicon library was denatured, diluted, and sequenced on an Illumina MiSeq platform using MiSeq Reagent Kit v3 (600 cycles) following the 2 × 300-bp paired-end sequencing protocol.

Phylogenetic and Statistical Analyses

The Illumina-generated sequence data were processed using the quantitative insights into microbial ecology software package (QIIME) v1.8.0 (43, 44). Sequences with quality score of Q20 and higher were assembled for paired ends using default parameters of PANDASEQ with a minimum overlap of 25 nucleotides and maximum of 100 nucleotides between forward and reverse reads (45, 46). The sequences were demultiplexed and quality trimmed using default parameters in QIIME script, *split_libraries_fastq.py* (47). The resulting total 7,040,079 sequences had an approximate read length of 500 bp. The filtered sequences were clustered into OTUs based on a 97% similarity threshold using UCLUST algorithm (48) and the chimeric sequences were removed by ChimeraSlayer (49). OTUs were picked by the *de novo* OTU picking method *pick_otus.py*. Representative sequences were aligned with PyNAST against Greengenes database (gg_13_8 release). Taxonomy was assigned to the identified OTUs using the basic local alignment search tool (BLAST) reference database and Greengenes taxonomy-mapping file. The script *make_phylogeny.py* was used to create phylogenetic trees with the FastTree program (50). Low-abundance OTUs with <2 counts were removed, and the remaining OTUs were used for downstream analysis. A total of 6,521,333 sequence reads (92.63%) were clustered into 11,357 OTUs (1,400,000 reads) for longitudinal mouse fecal samples; 10,710 OTUs (1,105,527 reads) for orthotopic mouse fecal samples; 248 OTUs (942,696 reads) for mouse tissue samples; 52,745 (2,706,209 reads) for human fecal samples; and 690 OTUs (366,901 reads) for human tissue samples.

The microbial relative abundance plots at all taxonomic levels were generated using biom, phyloseq, and pheatmap packages in R. OTUs with ≥0.1% abundance in at least one sample were considered for analysis, and <0.1% were binned into an "Other" category. The Mann–Whitney *U* test was used to compute significance between the health and disease cohorts, whereas significance within the samples over time was determined by the Wilcoxon signed rank test in R. Alpha diversity plots, such as richness estimators (observed OTUs, ACE, and Chao1) and diversity estimators (Shannon index, Simpson index, and PD), were generated using R-phyloseq and vegan. The data were rarefied by random subsampling without replacement to a depth of 2,500. This was based on minimum sequences in a dataset in order to normalize the read counts between samples. Two-tailed Student *t* test was also used when two groups were compared and ANOVA for three groups. β diversity PCoA plots were computed between cancer and control samples by weighted UniFrac distances, and significance was assessed by the Adonis test (PERMANOVA). LEfSe tool was used to identify differentially significant bacterial taxa between the cohorts with the Kruskal–Wallis test (51). *P* values ≤0.05 were considered statistically significant.

Quality Control

For adequate quality control, we used best practices of previously published studies (52–54). All the samples were collected using the standard sterile technique. We maintained consistency in DNA extraction techniques and reagents throughout. All PCR reagents were periodically checked for environmental contaminants using 16S universal primers. All qPCR reactions had appropriate controls (without template) to exclude bacterial DNA contamination.

Statistical Considerations for Tumor Size and Immunologic Analyses

Data are presented as mean ± standard error. Statistical significance in immune phenotyping studies and in measurements of tumor size was determined by the Student *t* test using GraphPad Prism 7 (GraphPad Software). *P* values <0.05 were considered significant.

Data Availability

Sequence data are available in the Sequence Read Archive database at the National Center for Biotechnology Information (Sequence Read Archive accession number SRP132007).

Disclosure of Potential Conflicts of Interest

G. Werba is a resident at George Washington University. D. Saxena is director at Periomics Care LLC and has ownership interest (including patents) in the same. No potential conflicts of interest were disclosed by the other authors.

Authors' Contributions

Conception and design: M. Hundeyin, C.P. Zambirinis, D. Saxena, G. Miller
Development of methodology: S. Pushalkar, M. Hundeyin, D. Daley, C.P. Zambirinis, A. Torres-Hernandez, A. Saxena, D. Saxena, G. Miller
Acquisition of data (provided animals, acquired and managed patients, provided facilities, etc.): M. Hundeyin, D. Daley, C.P. Zambirinis, A. Mishra, N. Mohan, B. Aykut, G. Werba, K. Zhang, Y. Guo, N. Akkad, S. Lall, B. Wadowski, J. Gutierrez, J.A. Kochen Rossi, J.W. Herzog, J. Leinwand, P.S. Taunk, S. Savadkar, A. Saxena, X. Li, R.B. Sartor, D. Saxena, G. Miller
Analysis and interpretation of data (e.g., statistical analysis, biostatistics, computational analysis): S. Pushalkar, M. Hundeyin, D. Daley, E. Kurz, A. Mishra, B. Aykut, M. Usyk, L.E. Torres, K. Zhang, Y. Guo, Q. Li, B. Wadowski, J.A. Kochen Rossi, J. Leinwand, W. Wang, P.S. Taunk, S. Savadkar, M. Janal, A. Saxena, X. Li, D. Saxena, G. Miller
Writing, review, and/or revision of the manuscript: S. Pushalkar, M. Hundeyin, C.P. Zambirinis, E. Kurz, A. Mishra, N. Mohan, B. Aykut, L.E. Torres, J. Leinwand, S. Savadkar, M. Janal, D. Cohen, D. Saxena, G. Miller
Administrative, technical, or material support (i.e., reporting or organizing data, constructing databases): S. Pushalkar, M. Hundeyin, D. Daley, E. Kurz, L.E. Torres, K. Zhang, Q. Li, B. Diskin, W. Wang, P.S. Taunk, S. Savadkar, D. Saxena, G. Miller
Study supervision: M. Hundeyin, J. Gutierrez, X. Li, D. Saxena, G. Miller
Other (microbiological studies, 16S rRNA sequencing): S. Pushalkar

Acknowledgments

This work was supported by NIH CA206105 (D. Saxena and G. Miller), CA168611 (G. Miller), CA155649 (G. Miller), DE025992 (D. Saxena), CA180277 (X. Li), CA175794 (A. Saxena), P40 OD010995 (R.B. Sartor), P30 DK034987 (R.B. Sartor), the Department of Defense Peer Reviewed Medical Research Program (G. Miller), the Lustgarten Foundation (D. Saxena and G. Miller), AACR-PanCan (G. Miller), the Panpaphian Association of America (C.P. Zambirinis), the National Pancreas Foundation (C.P. Zambirinis), Crohn's and Colitis Foundation of America (R.B. Sartor), NYU Provost Office Mega Grant Seed Fund Initiative (D. Saxena and X. Li), and the Irene and Bernard Schwartz Fellowship in GI Oncology (D. Daley). We thank the New York University Langone Medical Center (NYULMC) Histopathology Core Facility, the NYULMC Flow Cytometry Core Facility, the NYULMC Microscopy Core Facility, and the NYULMC BioRepository Center, each supported in part by the Cancer Center Support Grant P30CA016087 and by grant UL1 TR000038 from the National Center for the Advancement of Translational Science (NCATS). KC mice were a gift of D. Bar-Sagi and KPC mice were a gift of M. Philips, both from New York University.

The costs of publication of this article were defrayed in part by the payment of page charges. This article must therefore be hereby marked *advertisement* in accordance with 18 U.S.C. Section 1734 solely to indicate this fact.

Received October 9, 2017; revised January 3, 2018; accepted February 7, 2018; published first March 22, 2018.

REFERENCES

1. Siegel RL, Miller KD, Jemal A. Cancer statistics, 2016. CA Cancer J Clin 2016;66:7–30.
2. Zambirinis CP, Levie E, Nguy S, Avanzi A, Barilla R, Xu Y, et al. TLR9 ligation in pancreatic stellate cells promotes tumorigenesis. J Exp Med 2015;212:2077–94.
3. Ibrahim J, Nguyen AH, Rehman A, Ochi A, Jamal M, Graffeo CS, et al. Dendritic cell populations with different concentrations of lipid regulate tolerance and immunity in mouse and human liver. Gastroenterology 2012;143:1061–72.
4. Ochi A, Nguyen AH, Bedrosian AS, Mushlin HM, Zarbakhsh S, Barilla R, et al. MyD88 inhibition amplifies dendritic cell capacity to promote pancreatic carcinogenesis via Th2 cells. J Exp Med 2012;209:1671–87.
5. Zambirinis CP, Ochi A, Barilla R, Greco S, Deutsch M, Miller G. Induction of TRIF- or MYD88-dependent pathways perturbs cell cycle regulation in pancreatic cancer. Cell Cycle 2013;12:1153–4.
6. Seifert L, Werba G, Tiwari S, Giao Ly NN, Alothman S, Alqunaibit D, et al. The necrosome promotes pancreatic oncogenesis via CXCL1 and Mincle-induced immune suppression. Nature 2016;532:245–9.
7. Owyang C, Wu GD. The gut microbiome in health and disease. Gastroenterology 2014;146:1433–6.
8. Plottel CS, Blaser MJ. Microbiome and malignancy. Cell Host Microbe 2011;10:324–35.
9. Bultman SJ. Emerging roles of the microbiome in cancer. Carcinogenesis 2014;35:249–55.
10. Rutkowski MR, Stephen TL, Svoronos N, Allegrezza MJ, Tesone AJ, Perales-Puchalt A, et al. Microbially driven TLR5-dependent signaling governs distal malignant progression through tumor-promoting inflammation. Cancer Cell 2015;27:27–40.

11. Seifert L, Werba G, Tiwari S, Giao Ly NN, Nguy S, Alothman S, et al. Radiation therapy induces macrophages to suppress immune responses against pancreatic tumors in mice. Gastroenterology 2016;150:1659–72.e5.
12. Ino Y, Yamazaki-Itoh R, Shimada K, Iwasaki M, Kosuge T, Kanai Y, et al. Immune cell infiltration as an indicator of the immune microenvironment of pancreatic cancer. Br J Cancer 2013;108:914–23.
13. Daley D, Mani VR, Mohan N, Akkad N, Ochi A, Heindel DW, et al. Dectin 1 activation on macrophages by galectin 9 promotes pancreatic carcinoma and peritumoral immune tolerance. Nat Med 2017;23:556–67.
14. Daley D, Mani VR, Mohan N, Akkad N, Pandian G, Savadkar S, et al. NLRP3 signaling drives macrophage-induced adaptive immune suppression in pancreatic carcinoma. J Exp Med 2017;214:1711–24.
15. Hingorani SR, Wang L, Multani AS, Combs C, Deramaudt TB, Hruban RH, et al. Trp53R172H and KrasG12D cooperate to promote chromosomal instability and widely metastatic pancreatic ductal adenocarcinoma in mice. Cancer Cell 2005;7:469–83.
16. Garrett WS. Cancer and the microbiota. Science 2015;348:80–6.
17. Schwabe RF, Jobin C. The microbiome and cancer. Nat Rev Cancer 2013;13:800–12.
18. Clark CE, Hingorani SR, Mick R, Combs C, Tuveson DA, Vonderheide RH. Dynamics of the immune reaction to pancreatic cancer from inception to invasion. Cancer Res 2007;67:9518–27.
19. Zheng L, Xue J, Jaffee EM, Habtezion A. Role of immune cells and immune-based therapies in pancreatitis and pancreatic ductal adenocarcinoma. Gastroenterology 2013;144:1230–40.
20. Fukunaga A, Miyamoto M, Cho Y, Murakami S, Kawarada Y, Oshikiri T, et al. CD8+ tumor-infiltrating lymphocytes together with CD4+ tumor-infiltrating lymphocytes and dendritic cells improve the prognosis of patients with pancreatic adenocarcinoma. Pancreas 2004;28:e26–31.
21. De Monte L, Reni M, Tassi E, Clavenna D, Papa I, Recalde H, et al. Intratumor T helper type 2 cell infiltrate correlates with cancer-associated fibroblast thymic stromal lymphopoietin production and reduced survival in pancreatic cancer. J Exp Med 2011;208:469–78.
22. Hiraoka N, Onozato K, Kosuge T, Hirohashi S. Prevalence of FOXP3+ regulatory T cells increases during the progression of pancreatic ductal adenocarcinoma and its premalignant lesions. Clin Cancer Res 2006;12:5423–34.
23. Geller LT, Barzily-Rokni M, Danino T, Jonas OH, Shental N, Nejman D, et al. Potential role of intratumor bacteria in mediating tumor resistance to the chemotherapeutic drug gemcitabine. Science 2017;357:1156–60.
24. Tojo R, Suárez A, Clemente MG, de los Reyes-Gavilán CG, Margolles A, Gueimonde M, et al. Intestinal microbiota in health and disease: role of bifidobacteria in gut homeostasis. World J Gastroenterol 2014;20:15163–76.
25. Brown JH, Whitham TG, Morgan Ernest SK, Gehring CA. Complex species interactions and the dynamics of ecological systems: long-term experiments. Science 2001;293:643–50.
26. Nugent JL, McCoy AN, Addamo CJ, Jia W, Sandler RS, Keku TO. Altered tissue metabolites correlate with microbial dysbiosis in colorectal adenomas. J Proteome Res 2014;13:1921–9.
27. Sanapareddy N, Legge RM, Jovov B, McCoy A, Burcal L, Araujo-Perez F, et al. Increased rectal microbial richness is associated with the presence of colorectal adenomas in humans. ISME J 2012;6:1858–68.
28. Sivan A, Corrales L, Hubert N, Williams JB, Aquino-Michaels K, Earley ZM, et al. Commensal Bifidobacterium promotes antitumor immunity and facilitates anti-PD-L1 efficacy. Science 2015;350:1084–9.
29. Hingorani SR, Petricoin EF III, Maitra A, Rajapakse V, King C, Jacobetz MA, et al. Preinvasive and invasive ductal pancreatic cancer and its early detection in the mouse. Cancer Cell 2003;4:437–50.
30. Bedoret D, Wallemacq H, Marichal T, Desmet C, Quesada Calvo F, Henry E, et al. Lung interstitial macrophages alter dendritic cell functions to prevent airway allergy in mice. J Clin Invest 2009;119:3723–38.
31. Reikvam DH, Erofeev A, Sandvik A, Grcic V, Jahnsen FL, Gaustad P, et al. Depletion of murine intestinal microbiota: effects on gut mucosa and epithelial gene expression. PLoS One 2011;6:e17996.
32. Rehman A, Hemmert KC, Ochi A, Jamal M, Henning JR, Barilla R, et al. Role of fatty-acid synthesis in dendritic cell generation and function. J Immunol 2013;190:4640–9.
33. Hruban RH, Adsay NV, Albores-Saavedra J, Compton C, Garrett ES, Goodman SN, et al. Pancreatic intraepithelial neoplasia: a new nomenclature and classification system for pancreatic duct lesions. Am J Surg Pathol 2001;25:579–86.
34. Mi H, Muruganujan A, Casagrande JT, Thomas PD. Large-scale gene function analysis with the PANTHER classification system. Nat Protoc 2013;8:1551–66.
35. Ott SJ, Musfeldt M, Ullmann U, Hampe J, Schreiber S. Quantification of intestinal bacterial populations by real-time PCR with a universal primer set and minor groove binder probes: a global approach to the enteric flora. J Clin Microbiol 2004;42:2566–72.
36. Sunde PT, Olsen I, Gobel UB, Theegarten D, Winter S, Debelian GJ, et al. Fluorescence in situ hybridization (FISH) for direct visualization of bacteria in periapical lesions of asymptomatic root-filled teeth. Microbiology 2003;149:1095–102.
37. Thimm T, Tebbe CC. Protocol for rapid fluorescence in situ hybridization of bacteria in cryosections of microarthropods. Appl Environ Microbiol 2003;69:2875–8.
38. Choi YS, Kim YC, Baek KJ, Choi Y. In situ detection of bacteria within paraffin-embedded tissues using a digoxin-labeled DNA probe targeting 16S rRNA. J Vis Exp 2015;e52836.
39. Pushalkar S, Li X, Kurago Z, Ramanathapuram LV, Matsumura S, Fleisher KE, et al. Oral microbiota and host innate immune response in bisphosphonate-related osteonecrosis of the jaw. In J Oral Sci 2014;6:219–26.
40. Pushalkar S, Ji X, Li Y, Estilo C, Yegnanarayana R, Singh B, et al. Comparison of oral microbiota in tumor and non-tumor tissues of patients with oral squamous cell carcinoma. BMC Microbiol 2012;12:144.
41. Klindworth A, Pruesse E, Schweer T, Peplies J, Quast C, Horn M, et al. Evaluation of general 16S ribosomal RNA gene PCR primers for classical and next-generation sequencing-based diversity studies. Nucleic Acids Res 2013;41:e1.
42. Herlemann DPR, Labrenz M, Jurgens K, Bertilsson S, Waniek JJ, Andersson AF. Transitions in bacterial communities along the 2000 km salinity gradient of the Baltic Sea. ISME J 2011;5:1571–9.
43. Caporaso JG, Lauber CL, Walters WA, Berg-Lyons D, Huntley J, Fierer N, et al. Ultra-high-throughput microbial community analysis on the Illumina HiSeq and MiSeq platforms. ISME J 2012;6:1621–4.
44. Navas-Molina JA, Peralta-Sánchez JM, González A, McMurdie PJ, Vázquez-Baeza Y, Xu Z, et al. Advancing our understanding of the human microbiome using QIIME. Methods Enzymol 2013;531:371–444.
45. Masella AP, Bartram AK, Truszkowski JM, Brown DG, Neufeld JD. PANDAseq: paired-end assembler for illumina sequences. BMC Bioinformatics 2012;13:31.
46. Pircalabioru G, Aviello G, Kubica M, Zhdanov A, Paclet MH, Brennan L, et al. Defensive mutualism rescues NADPH oxidase inactivation in gut infection. Cell Host Microbe 2016;19:651–63.
47. Caporaso JG, Kuczynski J, Stombaugh J, Bittinger K, Bushman FD, Costello EK, et al. QIIME allows analysis of high-throughput community sequencing data. Nat Methods 2010;7:335–6.
48. Edgar RC. Search and clustering orders of magnitude faster than BLAST. Bioinformatics 2010;26:2460–1.
49. Haas BJ, Gevers D, Earl AM, Feldgarden M, Ward DV, Giannoukos G, et al. Chimeric 16S rRNA sequence formation and detection in Sanger and 454-pyrosequenced PCR amplicons. Genome Res 2011;21:494–504.
50. Price MN, Dehal PS, Arkin AP. FastTree: computing large minimum evolution trees with profiles instead of a distance matrix. Mol Biol Evol 2009;26:1641–50.
51. Segata N, Izard J, Waldron L, Gevers D, Miropolsky L, Garrett WS, et al. Metagenomic biomarker discovery and explanation. Genome Biol 2011;12:R60.
52. Goodrich JK, Di Rienzi SC, Poole AC, Koren O, Walters WA, Caporaso JG, et al. Conducting a microbiome study. Cell 2014;158:250–62.
53. Mukherjee S, Huntemann M, Ivanova N, Kyrpides NC, Pati A. Large-scale contamination of microbial isolate genomes by Illumina PhiX control. Stand Genomic Sci 2015;10:18.
54. Sinha R, Abnet CC, White O, Knight R, Huttenhower C. The microbiome quality control project: baseline study design and future directions. Genome Biol 2015;16:276.

CANCER DISCOVERY

AACR American Association for Cancer Research

The Pancreatic Cancer Microbiome Promotes Oncogenesis by Induction of Innate and Adaptive Immune Suppression

Smruti Pushalkar, Mautin Hundeyin, Donnele Daley, et al.

Cancer Discov Published OnlineFirst March 22, 2018.

Updated version	Access the most recent version of this article at: doi:10.1158/2159-8290.CD-17-1134

E-mail alerts	Sign up to receive free email-alerts related to this article or journal.
Reprints and Subscriptions	To order reprints of this article or to subscribe to the journal, contact the AACR Publications Department at pubs@aacr.org.
Permissions	To request permission to re-use all or part of this article, use this link http://cancerdiscovery.aacrjournals.org/content/early/2018/03/08/2159-8290.CD-17-1134. Click on "Request Permissions" which will take you to the Copyright Clearance Center's (CCC) Rightslink site.